

Quantum magnetism of ultra-cold fermion systems with the symplectic symmetry

Hsiang-Hsuan Hung,¹ Yupeng Wang,² and Congjun Wu¹

¹*Department of Physics, University of California, San Diego, CA 92093*

²*Beijing National Laboratory for Condensed Matter Physics, Institute of Physics, Chinese Academy of Sciences, Beijing 100080, P. R. China*

We numerically study quantum magnetism of ultra-cold alkali and alkaline-earth fermion systems with large hyperfine spin $F = \frac{3}{2}$, which are characterized by a generic $Sp(N)$ symmetry with $N = 4$. The methods of exact diagonalization (ED) and density-matrix-renormalization-group are employed for the large size one-dimensional (1D) systems, and ED is applied to a two-dimensional (2D) square lattice on small sizes. We focus on the magnetic exchange models in the Mott-insulating state at quarter-filling. Both 1D and 2D systems exhibit rich phase diagrams depending on the ratio between the spin exchanges J_0 and J_2 in the bond spin singlet and quintet channels, respectively. In 1D, the ground states exhibit a long-range-ordered dimerization with a finite spin gap at $J_0/J_2 > 1$, and a gapless spin liquid state at $J_0/J_2 \leq 1$, respectively. In the former and latter cases, the correlation functions exhibit the two-site and four-site periodicities, respectively. In 2D, various spin correlation functions are calculated up to the size of 4×4 . The Neel-type spin correlation dominates at large values of J_0/J_2 , while a 2×2 plaquette correlation is prominent at small values of this ratio. Between them, a columnar spin-Peierls dimerization correlation peaks. We infer the competitions among the plaquette ordering, the dimer ordering, and the Neel ordering in the 2D system.

PACS numbers: 71.10.Fd, 75.10.Jm, 71.10.Pm, 75.40.Mg

I. INTRODUCTION

The recent experimental progress on the ultracold Fermi gases with large hyperfine spin provides an exciting opportunity to investigate novel physical properties¹⁻⁴. In usual condensed matter systems, large spin is not considered particularly interesting because large values of spin suppress quantum fluctuations. For example, in transition metal oxides, a large spin on each cation site is usually referred as an effective spin S composed of $2S$ electrons by Hund's rule. The spin exchange between two cation sites at the leading order of the perturbation theory only involves swapping one pair of electrons regardless of how large S is. The variation of S_z is only ± 1 , thus increasing S reduces quantum fluctuations known as the $1/S$ -effect. In contrast, in ultracold fermion systems, the situation is dramatically different, in which large hyperfine spin enhances quantum fluctuations. Each atom moves as a whole object carrying a large hyperfine spin. Exchanging cold fermions can completely flip the entire hyperfine-spin configuration, and thus enhances quantum fluctuations. In other words, large spin physics in solid state systems is usually in the large S -limit, while in cold atom systems it is in the large N limit where N is the number of fermion components $2F + 1$ ³. We follow the convention in atomic physics to use F to denote the hyperfine spin of the atom.

Ultracold fermion systems with large hyperfine spins have aroused a great deal of theoretical interests. Early work studied the rich structures of the Fermi liquid theory⁵ and the Cooper pairing structures⁶. Considerable progress has been made in the simplest large hyperfine spin systems with $F = \frac{3}{2}$, whose possible candidate atoms are ¹³²Cs, ⁹Be, ¹³⁵Ba, ¹³⁷Ba and ²⁰¹Hg. These include both alkaline-earth-like atoms with zero

electron spin due to the fully filled electron shells, and non-alkaline-earth atoms with nonzero electron spins^{4,7,8}. In both cases, a generic $Sp(4)$, or, isomorphically, $SO(5)$ symmetry is proved without fine tuning. Such a high symmetry without fine-tuning is rare in both condensed matter and cold atom systems. It brings hidden degeneracy in the collective modes in the Fermi liquid theory⁹, fruitful patterns of quantum magnetism^{4,7,8,10,11} and Cooper pairing with large internal spin degrees of freedom^{8,12}. Further investigations in the community include the study of Mott insulating states¹³⁻¹⁸, Beth-ansatz solution^{19,20}, Kondo effect²¹, and the 4-fermion quartetting superfluidity²²⁻²⁴. Recently, $SU(N)$ models have been proposed for the alkaline-earth fermion atoms since their interactions are insensitive to their nuclear spins. It is a special case of the $Sp(N)$ model by further tuning interaction parameters of spin singlet and multiplet channels to be the same²⁵⁻²⁷. The possible ferromagnetic states have also been studied for the $SU(6)$ symmetric system of ¹⁷³Yb²⁸. A detailed summary is presented in a review Ref. [4] and a non-technique introduction is published at Ref. [3] by one of the authors. In a different context of heavy fermion systems, the effects of symplectic symmetry to quantum magnetism have also been studied in Ref. [29,30].

One dimensional (1D) systems are important for the study of strong correlation physics because of the dominant interaction effects. Furthermore, controllable analytical and numeric methods are available. In Ref. [11], one of the authors performed the bosonization method to study competing phases in 1D systems with $F = \frac{3}{2}$, including the gapless Luttinger liquid, spin gapped Luther-Emery liquid with Cooper pairing instability, and 4-fermion quartetting superfluid at incommensurate fillings. At commensurate fillings with strong repulsive in-

interactions, a charge gap opens and the systems become Mott-insulating. The gapless Luttinger liquid phase becomes a gapless spin liquid phase at quarter-filling and dimerized at half-filling, respectively⁴. The Luther-Emery phase becomes the gapped $Sp(4)$ dimer phase at quarter-filling and the on-site singlet phase at half-filling, respectively⁴.

On the other hand, the two dimensional (2D) $Sp(4)$ Heisenberg model is still far away from clear understanding. Such a system can bring fruitful intriguing features of quantum magnetism which do not exhibit in usual solid state systems. For example, in the special case of the $SU(4)$ symmetry, four particles are required to form an $SU(4)$ singlet, thus its quantum magnetism is characterized by the 4-site correlation beyond two sites. Such a state is the analogy to the three-quark color singlet baryon state in quantum chromodynamics. It is also the magnetism counterpart of the 4-fermion quartetting instability with attractive interactions⁴. Recently a magnetic phase diagram in a spatially anisotropic square lattice of the $Sp(4)$ quantum magnetism is provided by means of large- N field-theoretical approach³¹. A phase transition between the long-range Neel order state and the disordered valence bond solid phase is discovered by the perturbative renormalization group equations. However, the model on an isotropic square lattice is still unexplored. In particular, quantum Monte Carlo methods for this model suffer the notorious sign problem except in the special case where only the singlet bond exchange exists.

In this article, we present a systematic numerical study for the $Sp(4)$ Heisenberg model at quarter filling in both 1D systems with large sizes and 2D systems up to 4×4 by means of exact diagonalization techniques and the density matrix renormalization group (DMRG)^{32,33}. In 1D, we numerically show that the system exhibits two competing quantum phases: a long-range-ordered gapped dimer phase when the exchange interaction in the bond singlet channel (J_0) dominates over that in the quintet channel (J_2), and a gapless spin liquid phase otherwise. The $Sp(4)$ spin correlation functions are calculated, which shows that in the dimer phase the correlations have the 2-site periodicity, whereas in the gapless spin liquid phase they have the 4-sites periodicity. In 2D, our numerical simulations for small sizes indicate three different dominant correlations depending on the values of J_0/J_2 . We infer three competing phases: the Neel ordering, the plaquette ordering, and another possible phase of columnar dimer ordering, in the thermodynamic limit.

The rest of this article is organized as follows. In Sec. II, we introduce the Hamiltonian of spin- $\frac{3}{2}$ fermions which possesses the rigorous $Sp(4)$ symmetry, and a magnetic exchange model in the Mott-insulating state at quarter-filling. A self-contained introduction of the $Sp(4)/SO(5)$ algebra is given. Then we separate our main discussion into two parts: Sec. III for 1D and Sec. IV for 2D systems. In Sec. III A, we study the low-energy spectra of a finite size $Sp(4)$ chain with both

open and periodic boundary conditions. In Sec. III B, the DMRG calculation on the spin correlation functions are presented to identify the gapped $Sp(4)$ dimer phase and the gapless spin-liquid phase. In the second half part, we first analyze the 2×2 cluster in Sec. IV A and perform exact diagonalization on larger sizes to study the low-energy spectrum behavior in Sec. IV B. Then we display the calculations of the magnetic structure form factor in Sec. IV C, the dimer correlation in Sec. IV D and the plaquette-type correlation in Sec. IV E. We discuss the possible existence of the corresponding orderings. Conclusions are made in the last section. At the end of this paper, we present a brief and self-contained introduction to the representation theory of Lie group in Appendix A to C.

II. MODEL HAMILTONIAN AND THE HIDDEN $Sp(4)$ SYMMETRY

A. The spin- $\frac{3}{2}$ Hubbard model

We start with the generic one-band Hubbard model loaded with spin- $\frac{3}{2}$ fermions. By neglecting long-range Coulomb interactions, only onsite interactions are considered in the Hubbard model. Due to Pauli's exclusion principle, the spin wavefunctions of two onsite fermions have to be antisymmetric. The total spin of two onsite spin- $\frac{3}{2}$ fermions can only be either singlet ($S_T = 0$) or quintet ($S_T = 2$). We assign an independent interaction parameter U_0 (singlet) and U_2 (quintet), respectively, to each channel. The Hamiltonian reads

$$H = -t \sum_{\langle ij \rangle, \sigma} (\psi_{i\sigma}^\dagger \psi_{j\sigma} + h.c.) - \mu \sum_{i\sigma} \psi_{i\sigma}^\dagger \psi_{i\sigma} + U_0 \sum_i P_0^\dagger(i) P_0(i) + U_2 \sum_{i,m=-2,\dots,2} P_{2m}^\dagger(i) P_{2m}(i), \quad (1)$$

where $\langle ij \rangle$ denotes the nearest neighboring hopping; σ represents four spin flavors $F_z = \pm\frac{3}{2}, \pm\frac{1}{2}$; P_0^\dagger and P_{2m}^\dagger are the singlet and quintet pairing operators defined through Clebsch-Gordon coefficients as

$$P_0^\dagger(i) = \sum_{\alpha\beta} \langle 00 | \frac{3}{2} \frac{3}{2} \alpha\beta \rangle \psi_\alpha^\dagger(i) \psi_\beta^\dagger(i), \\ P_{2m}^\dagger(i) = \sum_{\alpha\beta} \langle 2m | \frac{3}{2} \frac{3}{2} \alpha\beta \rangle \psi_\alpha^\dagger(i) \psi_\beta^\dagger(i). \quad (2)$$

The actual symmetry of Eq. 1 is much larger than the $SU(2)$ symmetry: it has a hidden and exact $Sp(4)$, or, isomorphically, $SO(5)$ symmetry. The $Sp(4)$ algebra can be constructed as follows. For the 4-component fermions, there exist 16 bases for the 4×4 Hermitian matrices $M_{\alpha\beta}(\alpha, \beta = \pm\frac{3}{2}, \pm\frac{1}{2})$. They serve as matrix kernels for the bi-linear operators, i.e., $\psi_\alpha^\dagger M_{\alpha\beta} \psi_\beta$, in the particle-hole channel. The density and 3-component

spin F_x, F_y, F_z operators *do not* form a complete set. The other 12 operators are built up as high rank spin tensors, including 5-component spin-quadrupoles and 7-component spin-octupoles. The matrix kernels of the spin-quadrupole operators are defined as

$$\begin{aligned}\Gamma^1 &= \frac{1}{\sqrt{3}}(F_x F_y + F_y F_x), \quad \Gamma^2 = \frac{1}{\sqrt{3}}(F_z F_x + F_x F_z), \\ \Gamma^3 &= \frac{1}{\sqrt{3}}(F_z F_y + F_y F_z), \quad \Gamma^4 = (F_z^2 - \frac{5}{4}), \\ \Gamma^5 &= \frac{1}{\sqrt{3}}(F_x^2 - F_y^2),\end{aligned}\quad (3)$$

which anti-commute with each other, and thus form a basis of the Dirac- Γ matrices. The matrix kernels of 3 spin and 7 spin-octupole operators together are generated from the commutation relations among the 5 Γ -matrices as

$$\Gamma^{ab} = -\frac{i}{2}[\Gamma^a, \Gamma^b] \quad (1 \leq a, b \leq 5). \quad (4)$$

Consequently, these 16 bilinears can be classified as

$$n = \psi_\alpha^\dagger \psi_\alpha, \quad n_a = \frac{1}{2} \psi_\alpha^\dagger \Gamma_{\alpha\beta}^a \psi_\beta, \quad L_{ab} = -\frac{1}{2} \psi_\alpha^\dagger \Gamma_{\alpha\beta}^{ab} \psi_\beta, \quad (5)$$

where n is the density operator; n_a 's are 5-component spin-quadrupole operators; L_{ab} 's are 10-component spin and spin-octupole operators^{4,10}. Reversely the spin $SU(2)$ generators $F_{x,y,z}$ can be written as $F_+ = \sqrt{3}(-L_{34} + iL_{24}) - (L_{12} + iL_{25}) + i(L_{13} + iL_{35})$ and $F_z = L_{23} + 2L_{15}$.

The 15 operators of n_a and L_{ab} together span the $SU(4)$ algebra. Among them, the 10 L_{ab} operators are spin tensors with odd ranks, and thus time-reversal (TR) odd, while the 5-component n_a 's are TR even. The TR odd operators of L_{ab} form a closed sub-algebra of $Sp(4)$. The 4-component spin- $\frac{3}{2}$ fermions form the fundamental spinor representation of the $Sp(4)$ group. In contrast, the TR even operators of n_a do not form a closed algebra, but transform as a 5-vector under the $Sp(4)$ group. In other words, $Sp(4)$ is isomorphic to $SO(5)$. But rigorously speaking, the fermion spinor representations of $Sp(4)$ are not representations of $SO(5)$. Their relation is the same as that between $SU(2)$ and $SO(3)$. Below we will use the terms of $Sp(4)$ and $SO(5)$ interchangeably. The $SO(5)$ symmetry of Eq. 1 can be intuitively understood as follows. The 4-component fermions are equivalent to each other in the kinetic energy term, which has an obvious $SU(4)$ symmetry. Interactions break the $SU(4)$ symmetry down to $SO(5)$. The singlet and quintet channels form the identity and 5-dimensional vector representations for the $SO(5)$ group, respectively, thus Eq. 1 is $SO(5)$ invariant without any fine-tuning.

B. Magnetic exchanges at quarter-filling

Mott-insulating states appear at commensurate fillings with strong repulsive interactions. We focus on the magnetic exchange at quarter filling, *i.e.*, one fermion per

site. The Heisenberg type exchange model has been constructed in Ref. [7] through the second-order perturbation theory. For each bond, the exchange energies are $J_0 = \frac{4t^2}{U_0}$ for the bond spin singlet channel, $J_2 = \frac{4t^2}{U_2}$ for the bond spin quintet channel, and $J_1 = J_3 = 0$ for the bond spin triplet and septet channels, respectively. This exchange model can be written in terms of bi-linear, bi-quadratic and bi-cubic Heisenberg exchange and the Hamiltonian reads as

$$H_{ex} = \sum_{\langle i,j \rangle} a(\vec{F}_i \cdot \vec{F}_j) + b(\vec{F}_i \cdot \vec{F}_j)^2 + c(\vec{F}_i \cdot \vec{F}_j)^3, \quad (6)$$

where $a = -\frac{1}{96}(31J_0 + 23J_2)$, $b = \frac{1}{72}(5J_0 + 17J_2)$ and $c = \frac{1}{18}(J_0 + J_2)$ and $F_{x,y,z}$ are usual 4×4 spin operators. Eq. 6 can be simplified into a more elegant form with the explicitly $SO(5)$ symmetry⁴ as

$$\begin{aligned}H_{ex} &= \sum_{\langle i,j \rangle} \left\{ \sum_{1 \leq a < b \leq 5} \frac{J_0 + J_2}{4} L_{ab}(i) L_{ab}(j) \right. \\ &\quad \left. + \frac{3J_2 - J_0}{4} \sum_{a=1}^5 n_a(i) n_a(j) \right\}. \quad (7)\end{aligned}$$

In the $SO(5)$ language, there are two diagonal operators commuting with each other and read as

$$\begin{aligned}L_{15} &= \frac{1}{2}(n_{\frac{3}{2}} + n_{\frac{1}{2}} - n_{-\frac{1}{2}} - n_{-\frac{3}{2}}), \\ L_{23} &= \frac{1}{2}(n_{\frac{3}{2}} - n_{\frac{1}{2}} + n_{-\frac{1}{2}} - n_{-\frac{3}{2}}).\end{aligned}\quad (8)$$

Corresponding to the spin language, each singlet-site basis state can be labeled in terms of these two quantum numbers as $|F_z\rangle = |L_{15}, L_{23}\rangle$: $|\pm \frac{3}{2}\rangle = |\pm \frac{1}{2}, \pm \frac{1}{2}\rangle$ and $|\pm \frac{1}{2}\rangle = |\pm \frac{1}{2}, \mp \frac{1}{2}\rangle$. For an arbitrary many-body state, $L_{15}^{tot} = \sum_i L_{15}(i)$ and $L_{23}^{tot} = \sum_i L_{23}(i)$ are good quantum numbers (similar to that $F_z^{tot} = \sum_i F_z(i)$ is conserved in $SU(2)$ cases) and can be applied to reduce dimensions of the Hilbert space in practical numerical calculations.

There exist two different $SU(4)$ symmetries of Eq. 7 in two special cases. At $J_0 = J_2 = J$, *i.e.*, $U_0 = U_2$, it reduces to the $SU(4)$ Heisenberg model with each site in the fundamental representation

$$H = \sum_{\langle i,j \rangle} \frac{J}{2} \{ L_{ab}(i) L_{ab}(j) + n_a(i) n_a(j) \}. \quad (9)$$

Below we denote this symmetry as $SU(4)_A$. In this case, there is an additional good quantum number n_4 ,

$$n_4 = \frac{1}{2}(n_{\frac{3}{2}} - n_{\frac{1}{2}} - n_{-\frac{1}{2}} + n_{-\frac{3}{2}}). \quad (10)$$

This $SU(4)$ model is equivalent to the Kugel-Khomskii type model^{34,35} and is used to study the physics with interplay between orbital and spin degree of freedom.³⁶⁻³⁸ On the other hand, at $J_2 = 0$, *i.e.*, $U_2 \rightarrow +\infty$, Eq. 7 has another $SU(4)$ symmetry in the bipartite lattice, which

is denoted $SU(4)_B$ below. In this case, we perform the particle-hole transformation to one sublattice but leave the other sublattice unchanged. The particle-hole transformation is defined as $\psi_\alpha \rightarrow R_{\alpha\beta} \psi_\beta^\dagger$ where R is the charge conjugation matrix

$$R = \begin{pmatrix} 0 & i\sigma_2 \\ i\sigma_2 & 0 \end{pmatrix}. \quad (11)$$

Under this operation, the fundamental representation transforms to anti-fundamental representation whose $Sp(4)$ generators and vectors become $L'_{ab} = L_{ab}$ and $n'_a = -n_a$. Thus Eq. 7 can be recast to

$$H = \sum_{\langle i,j \rangle} \frac{J}{2} (L'_{ab}(i) L_{ab}(j) + n'_a(i) n_a(j)), \quad (12)$$

which is $SU(4)$ invariant again.

These two $SU(4)$ symmetries have very different physical properties. In the case of $SU(4)_A$, two sites are not enough to form an $SU(4)$ singlet. It at least needs four sites to form an $SU(4)$ singlet as $\epsilon_{\alpha\beta\gamma\delta} \psi_\alpha^\dagger(1) \psi_\beta^\dagger(2) \psi_\gamma^\dagger(3) \psi_\delta^\dagger(4)$, where $\epsilon_{\alpha\beta\gamma\delta}$ is the rank-4 fully antisymmetric tensor. Thus quantum magnetism of Eq. 7 at $J_0 = J_2$ is characterized by four-site correlations. The ground state of such a system on a 2D square lattice was conjectured to be a plaquette $SU(4)$ singlet state without magnetic long-ranged ordering.^{37,39} On the other hand, for the $SU(4)_B$ case, two sites can form an $SU(4)$ singlet as $R_{\alpha\beta} \psi_\alpha^\dagger(1) \psi_\beta^\dagger(2)$. In the 2D square lattice, a long-ranged Neel order is identified by quantum Monte Carlo simulations⁴⁰ and large N limit.⁴¹ The square of the staggered magnetization is numerically given as $m_s = 0.091$, which is much smaller than that of the $SU(2)$ Neel order state.

III. QUANTUM MAGNETISM IN THE 1D CHAINS

We start our discussion on the 1D chain. The phase diagram of the 1D spin- $\frac{3}{2}$ Hubbard model has been studied by one of the author using the method of bosonization^{4,11}. At the commensurate quarter-filling (one particle per site) with purely repulsive interactions ($U_0 > 0, U_2 > 0$), the $4k_f$ -Umklapp term opens a charge gap as $K_c < \frac{1}{2}$. In this case, the physics is captured by the exchange model of Eq. 7. It has been found that in the regime of $J_0/J_2 > 1$ dimerization of spin Perierls order is present, whereas it is a gapless spin liquid phase at $J_0/J_2 \leq 1$ (see Fig. 1)¹¹. In the following, we use exact diagonalization methods and DMRG not only identify these two competing phases but also demonstrate the ground state profiles and 4-site periodicities in spin-spin correlations.

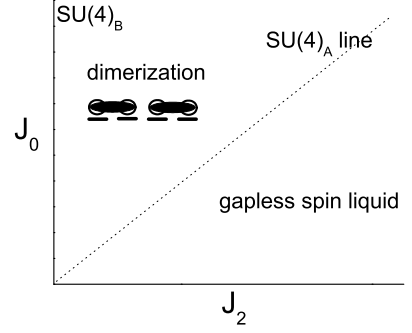


FIG. 1: Phase diagram of the 1D chain in terms of the singlet and quintet channel interaction J_0 and J_2 . In this context, θ is the angle defined by $\theta = \tan^{-1}(J_0/J_2)$. The $SU(4)_A$ type ($\theta = 45^\circ$) denoted by the dot line belongs to the gapless spin liquid state whereas $SU(4)_B$ along $J_2 = 0$. The phase boundary separating the dimerization phase and the gapless liquid state is the $SU(4)_A$ line.

A. Exact diagonalization on low energy spectra

In this subsection, we apply the exact diagonalization technique to study the 1D $Sp(4)$ spin- $\frac{3}{2}$ chains with nearest neighbor exchange interactions described by Eq. 7. We only consider the case of the site number $N = 4m$. For convenience, we set $J_0 = \sqrt{2} \sin \theta$ and $J_2 = \sqrt{2} \cos \theta$. Regardless of θ and sizes N , the ground states (GS) only exist in the $(L_{15}^{tot}, L_{23}^{tot}) = (0, 0)$ sector and are unique with $C = 0$, where C denotes the $Sp(4)$ Casimir of the entire system and is expressed in terms of the $Sp(4)$ generators as

$$C = \sum_{1 \leq a < b \leq 5} \left\{ \sum_i L_{ab}(i) \right\}^2. \quad (13)$$

In addition to L_{15}^{tot} and L_{23}^{tot} , the Casimir C is also a conserved quantity in the $Sp(4)$ system, analogous to the total spin in $SU(2)$ systems. Each energy eigenstate can be labeled by C and further identified the dimension of the representation (degeneracy). As shown in the table II in the Appendix, while $C = 0$, the state is an $Sp(4)$ singlet and unique whereas while $C > 0$ the state is multiplet and has degeneracy which is equal to the dimension of the associated representation.

In Fig. 2 (a) and (b), the ground state and low excited states with 12 sites are presented using open and periodic boundary conditions, respectively. The GS as varying θ angles is always an $Sp(4)$ singlet, which becomes an $SU(4)$ singlet at $\theta = 45^\circ$ ($SU(4)_A$) and $\theta = 90^\circ$ ($SU(4)_B$) for both boundary conditions. For the low energy excited states, we first look at the regime of $45^\circ < \theta < 90^\circ$, i.e., $J_0 > J_2$. With open boundary conditions (OBC), the lowest excited states (LES) are the $Sp(4)$ 5-vector states with the quadratic Casimir $C = 4$. The next lowest excited states (NLES) are 10-fold degenerate and belong to the 10-dimensional (10d) $Sp(4)$ adjoint representation with $C = 6$. The LES and NLES merge at both of the

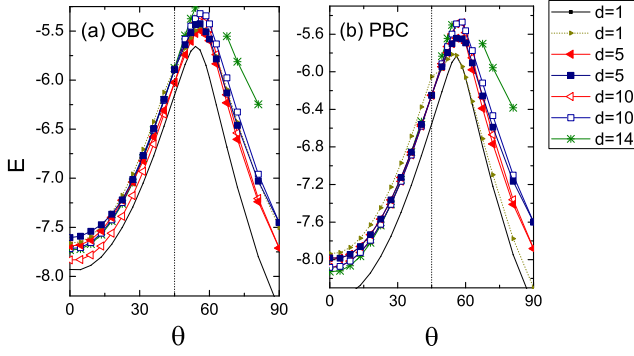


FIG. 2: The exact diagonalization on 1D chain with 12 sites for (a) open and (b) periodic boundary conditions. The dispersion of the ground state and low excited states, and the dimensions d of their corresponding representations of the $Sp(4)$ group are shown.

$SU(4)_A$ ($\theta = 45^\circ$) and $SU(4)_B$ ($\theta = 90^\circ$) points, and become 15-fold degenerate. This is the $SU(4)$ adjoint representation with $C = 8$. With periodic boundary conditions (PBC), the 5-vector and the 10-fold states behave similarly as before. However, a marked difference is that a new $Sp(4)$ singlet state appears as the LES at $50^\circ < \theta < 90^\circ$, which becomes higher than the 5-vector states only very close to 45° . In particular, it is nearly degenerate with the ground state (which is the lowest $Sp(4)$ singlet) at $\theta = 50^\circ \sim 60^\circ$. In the regime of $0^\circ < \theta < 45^\circ$, i.e., $J_2 > J_0$ the excited states are many $Sp(4)$ multiplets with energies close to each other. With OBC, the LESs form the 10d $Sp(4)$ adjoint representation. For the PBC case, the 14-dimensional symmetric tensor representation of $Sp(4)$ competes with the 10d adjoint one.

The appearance of two nearly degenerate $Sp(4)$ singlets at $50^\circ < \theta < 90^\circ$ with PBC and their disappearance with OBC can be understood by the dimerization instability. The dimerization and the spin gapped ground state was shown in the bosonization analysis at $45^\circ < \theta < 90^\circ$ ¹¹. In the thermodynamic limit, the ground state has double degeneracy corresponding to two different dimer configurations, both spontaneously breaking translational symmetry. The OBC favors only one of the dimer configurations, but disfavors the other due to one bond breaking. In the finite system with PBC, the two dimer configurations tunnel between each other, which gives rise to two nearly degenerate $Sp(4)$ singlet states. We further calculate the gap between them, denoted by Δ_{ss} , at $\theta > 45^\circ$ by using exact diagonalization under PBC up to 16 sites.

As presented in Fig. 3, Δ_{ss} disappears in the finite size scaling due to the twofold degeneracy. On the other hand, the existence of the spin gap in this parameter regime is presented in Fig. 4 by DMRG simulation in Sec. III B below. The original Lieb-Schultz-Mattis theorem⁴² was proved that for the $SU(2)$ case, the GS of half-integer spin chains with translational and rotational symmetries is gapless, or gapped with breaking translational symme-

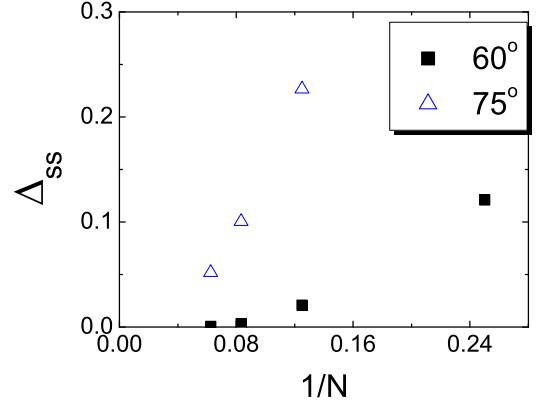


FIG. 3: Exact diagonalization results on the $Sp(4)$ singlet-singlet gap with $J_0 > J_2$ and periodic boundary conditions ($\theta = 60^\circ$ and 75° with $N = 8, 12$ and 16). Finite size scaling shows the vanishing of the singlet-singlet gap Δ_{ss} .

try. It is interesting to observe that our results of the $Sp(4)$ spin chain also agree with this theorem. The nature of the GS in the parameter regime $0^\circ < \theta < 45^\circ$ will be discussed in Sec. III B.

B. DMRG simulations on $Sp(4)$ spin chain

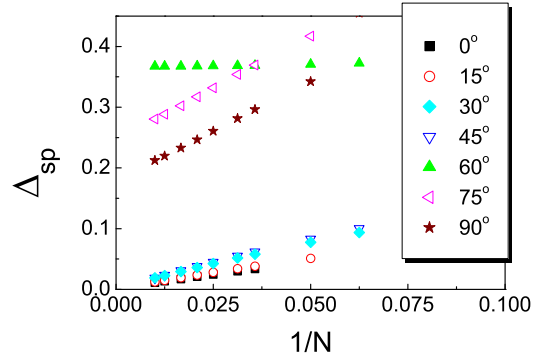


FIG. 4: The finite size scaling of the spin gap Δ_{sp} of the $Sp(4)$ spin chain vs $1/N$ at various values of θ . θ is defined as $\theta = \tan^{-1}(J_0/J_2)$ and N is the system size.

In this subsection, we present the DMRG calculations on the ground state properties of the $Sp(4)$ chain up to 80 sites with OBC. We first present the spin gap Δ_{sp} in Fig. 4, which is defined as the energy difference between the ground state and the lowest $Sp(4)$ multiplet.

For chains with even number of sites, the GS is obtained with quantum number $L_{15}^{tot} = L_{23}^{tot} = 0$, and any $Sp(4)$ multiplet contains the states with quantum numbers ($L_{15}^{tot} = \pm 1, L_{23}^{tot} = 0$) and ($L_{15}^{tot} = 0, L_{23}^{tot} = \pm 1$). States with the same values of ($L_{15}^{tot}, L_{23}^{tot}$) may belong to different $Sp(4)$ representations, which can be distinguished by their $Sp(4)$ Casimir. Practically, we only need to calculate these sectors with low integer values

of $(L_{15}^{tot}, L_{23}^{tot})$ to determine the spin gaps. For the cases of $\theta > 45^\circ$, i.e., $(J_2/J_0 < 1)$, Δ_{sp} s saturate to nonzero values as $1/N \rightarrow 0$, indicating the opening of spin gaps. On the other hand, Δ_{sp} 's vanish at $\theta \leq 45^\circ$, which shows that the ground state is gapless. These results agree with the bosonization analysis¹¹, which shows that the phase boundary is at $\theta = 45^\circ$ with the $SU(4)_A$ symmetry, which is also gapless. This gapless $SU(4)_A$ line was also studied before in Ref. [43,44].

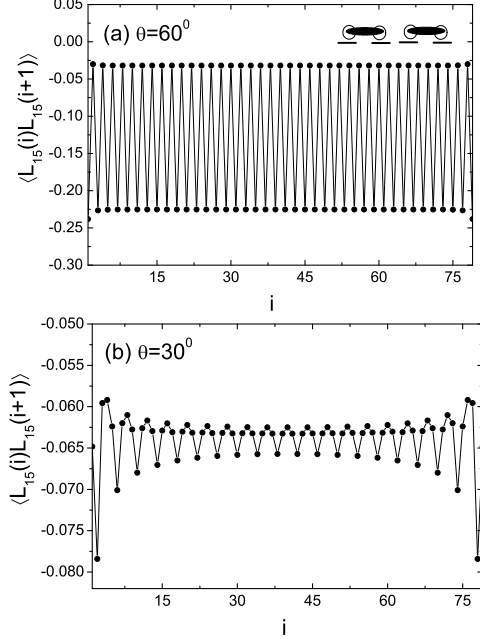


FIG. 5: The NN correlation of $\langle L_{15}(i)L_{15}(i+1) \rangle$ with open boundary conditions for (a) $\theta = 60^\circ$ and (b) $\theta = 30^\circ$, respectively. The dimer ordering is long-ranged in (a). Note the 2-site periodicity in (a) and the 4-site periodicity in (b).

To further explore the ground state profile, we calculate the nearest neighbor (NN) correlation functions of the $Sp(4)$ generators for a chain of 80 sites. This correlation function is similar to the bonding strength and defined as $\langle X(i)X(i+1) \rangle$, where X are $Sp(4)$ generators. We present the result of $\langle L_{15}(i)L_{15}(i+1) \rangle$ in Fig. 5, and the correlation functions of other generators should be the same due to the $Sp(4)$ symmetry. The open boundary induces characteristic oscillations. At $\theta = 60^\circ$, i.e., $J_0/J_2 = \sqrt{3}$, $\langle L_{15}(i)L_{15}(i+1) \rangle$ exhibits the dominant dimer pattern, which does not show noticeable decay from the edge to the middle of the chain. This means that the dimerization is long-range-ordered in agreement with the bosonization analysis⁴. In contrast, at $\theta = 30^\circ$, i.e., $J_2/J_0 = \sqrt{3}$, $\langle L_{15}(i)L_{15}(i+1) \rangle$ exhibits a characteristic power-law decay with 4-site periodicity oscillations. The 4-site periodicity is also observed at other θ 's for $\theta \leq 45^\circ$, same as ones presented in the bosonization analysis.

We follow the definition for the dimer order parameter

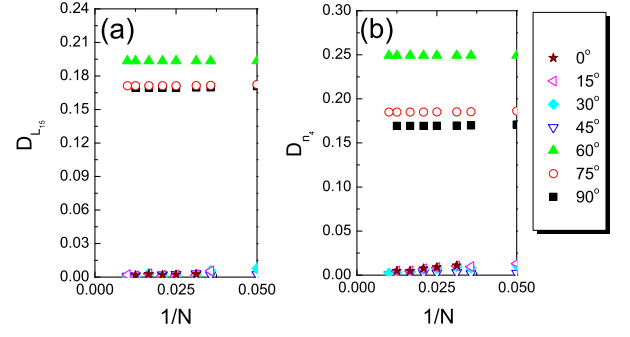


FIG. 6: The finite size scaling for the dimer order parameters (a) $D_{L_{15}}$ and (b) D_{n_4} vs $1/N$ at various θ 's.

in Ref. [45,46] as

$$D_X = |\langle X(\frac{N}{2} - 1)X(\frac{N}{2}) \rangle - \langle X(\frac{N}{2})X(\frac{N}{2} + 1) \rangle|. \quad (14)$$

As shown previously, X s are $Sp(4)$ generators and vectors in the $Sp(4)$ spin chain. Without loss of generality, we choose two non-equivalent operators as $X = L_{15}$ and n_4 for $Sp(4)$ generators and vectors, respectively. The open boundary conditions provide an external field to pin down the dimer orders. The finite size scaling of the dimer orders of the two middle bonds is presented in Fig. 6 (a) and (b) at various values of θ , respectively. It is evident that in the regime of $\theta > 45^\circ$ both of $D_{L_{15}}$ and D_{n_4} remain finite as $1/N \rightarrow 0$ whereas for $\theta \leq 45^\circ$ the dimer order parameters vanish. We conclude that the ground state is the dimer phase for $J_0/J_2 > 1$.

Next we present the two point correlation functions of $\langle X(i)X(j) \rangle$, where X is L_{15} and n_4 , in Fig. 7 (a) and (b), respectively. At $\theta > 45^\circ$, say, $\theta = 60^\circ$, both correlation functions show exponential decay due to the dimerization. In the spin liquid regime of $\theta \leq 45^\circ$, i.e., $J_2 \geq J_0$, however, all the correlation functions exhibit the power-law behavior and the same $2k_f$ oscillations with the 4-site period. Their asymptotic behavior can be written as

$$\langle X(i_0)X(i) \rangle \propto \frac{\cos \frac{\pi}{2}|i - i_0|}{|i - i_0|^\kappa}. \quad (15)$$

Along the $SU(4)_A$ line ($\theta = 45^\circ$), the correlations of L_{15} and n_4 are degenerate. The power can be fitted as $\kappa \approx 1.52$, which is in good agreement with the value of 1.5 from bosonization analysis and numerical studies^{11,43,44,47}. As θ is away from 45° , the $SU(4)$ symmetry is broken. For the correlations of L_{15} , the values of κ decrease as decreasing θ , which can be fitted as $\kappa = 1.41, 1.34, 1.30$ for $\theta = 30^\circ, 15^\circ, 0^\circ$, respectively. On the other hand, for the correlations of n_4 , the values of κ can be fitted as $\kappa = 1.55, 1.65, 1.60$ for $\theta = 30^\circ, 15^\circ, 0^\circ$, respectively. We also perform the Fourier transforms of the correlations of $\langle L_{15}(i_0)L_{15}(i) \rangle$, $S(q)$, and present the

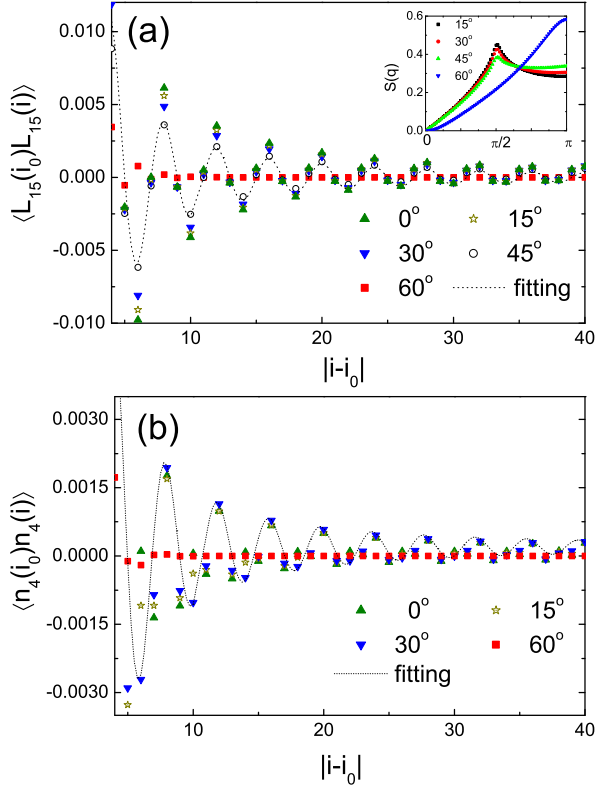


FIG. 7: (a) The two point correlations $\langle L_{15}(i_0)L_{15}(i) \rangle$ at $\theta = 0^\circ, 15^\circ, 30^\circ, 45^\circ$ and 60° . The dot line is plotted by the fitting result using $\cos(x\pi/2)/x^{1.52}$. The reference point $i_0 (= 40)$ is the most middle site of the chain ($N = 80$). The inset indicates that all $S(q)$ for $\theta \leq 45^\circ$ have peaks located at $q = 41\pi/81 \sim \pi/2$ whereas π for $\theta = 60^\circ$. (b) $\langle n_4(i_0)n_4(i) \rangle$ at $\theta = 0^\circ, 15^\circ, 30^\circ$ and 60° and the fitting uses $\kappa = 1.55$.

results in the inset of Fig. 7 (a). $S(q)$ is defined as

$$S(q) = \sum_{i,j} e^{iq(r_i - r_j)} \langle L_{15}(r_i)L_{15}(r_j) \rangle \quad (16)$$

and $q = m\pi/(N+1)$, where $m = 1, 2, \dots, N$ are integers for OBC. Clearly, in the regime of $\theta \leq 45^\circ$ all the peaks are located at $q = 41\pi/81 \sim \pi/2$, indicating a $2k_f$ charge density wave. On the other hand, $S(q)$ at $\theta = 60^\circ$ appears a peak at π , which denotes a $4k_f$ charge density wave and is characteristic of the dimerization phase.

IV. THE $Sp(4)$ MAGNETISM IN 2D SQUARE LATTICE WITH SMALL SIZES

The quantum magnetism of Eq. 7 in 2D is a very challenging problem. Up to now, a systematic study is still void. In the special case of the $SU(4)_B$ line, i.e. $J_2 = 0$, in the square lattice, quantum Monte-Carlo simulations are free of the sign problem, which shows the long-range-Neel ordering but with very small Neel moments $n_4 = (-)^i L_{15} = (-)^i L_{23} \approx 0.05^{40}$. This result agrees

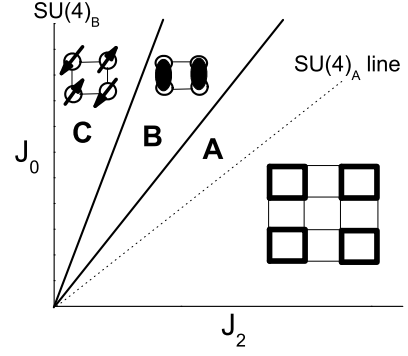


FIG. 8: Speculated phase diagram of the 2D $Sp(4)$ spin-3/2 systems at quarter filling from Ref. [4]. $\theta = \tan^{-1}(J_0/J_2)$. The $SU(4)_A$ type drawn by the dot line is at $J_0 = J_2$ ($\theta = 45^\circ$) whereas $SU(4)_B$ at $J_2 = 0$ ($\theta = 90^\circ$). Bold letters **A**, **B**, and **C** represent the plaquette, columnar dimerized and Neel order states, respectively.

with the previous large- N analysis⁴⁸. The Goldstone manifold is $CP(3) = U(4)/[U(1) \otimes U(3)]$ with 6 branches of spin-waves. On the other hand, on the $SU(4)_A$ line with $J_0 = J_2$, an exact diagonalization study on the 4×4 sites shows the evidence of the four-site $SU(4)$ singlet plaquette ordering³⁷. Large size simulations are too difficult to confirm this result. On the other hand, a variational wavefunction method based on the Majorana representation of spin operators suggests a spin-liquid state at the $SU(4)_A$ line⁴⁹. Recently, Chen *et al.*⁷ constructed an $SU(4)$ Majumdar-Ghosh model in a two-leg spin-3/2 ladder whose ground state is solvable exhibiting this plaquette state. An $SU(4)$ resonant plaquette model in 3D have also been constructed^{8,50}.

Based on these available knowledge, a speculated phase diagram was provided in Ref. [4] as shown in Fig. 8. The Neel order state **C** is expected to extend to a region with finite J_2 instead of only along the $J_2 = 0$ line. Furthermore, the plaquette order phase **A** exists not only along the $SU(4)_A$ line but also covers a finite range including $\theta = 45^\circ$. Between **A** and **C**, there exists an intermediate phase **B** which renders ordered dimerizations which are two-sites spin singlets. However, these features have not been tested due to the lack of controllable analytic and numeric methods for 2D strongly correlation systems. For example, quantum Monte Carlo methods suffer notorious sign problems at $J_2 \neq 0$.

In this section, we begin with the cluster of 2×2 whose ground states can be solved analytically. Then we perform exact diagonalization (ED) methods for the case of 4×4 sites and analyze the associated GS profiles for different values of θ . Even though the size that we are studying is still small to draw any conclusion for the thermodynamic limit, it provides valuable information on the ground state properties.

A. The 2×2 cluster

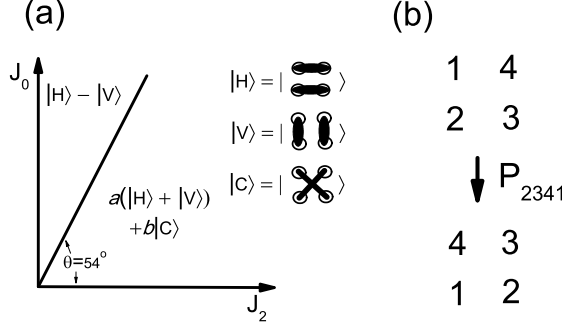


FIG. 9: (a) The GS wavefunctions of the 2×2 cluster at various θ . a and b are coefficients depending on θ and the thick bonds denote the two-site $Sp(4)$ spin singlet states. (b) The position indices before and after the permutation P_{2341} .

We begin with the 2×2 cluster, whose ground states can be solved analytically for all the values of θ . Such a system contains three $Sp(4)$ singlets, and the ground states can be expanded in this singlet subspace. These $Sp(4)$ singlets can be conveniently represented in terms of the dimer states with the horizontal, vertical, and cross diagonal configurations depicted in Fig. 9 (a) as

$$\begin{aligned} |H\rangle &= \frac{1}{4} R_{\alpha\beta} \psi_{\alpha}^{\dagger}(4) \psi_{\beta}^{\dagger}(1) R_{\gamma\delta} \psi_{\gamma}^{\dagger}(2) \psi_{\delta}^{\dagger}(3) |\Omega\rangle, \\ |V\rangle &= \frac{1}{4} R_{\alpha\beta} \psi_{\alpha}^{\dagger}(1) \psi_{\beta}^{\dagger}(2) R_{\gamma\delta} \psi_{\gamma}^{\dagger}(3) \psi_{\delta}^{\dagger}(4) |\Omega\rangle, \\ |C\rangle &= \frac{1}{4} R_{\alpha\beta} \psi_{\alpha}^{\dagger}(1) \psi_{\beta}^{\dagger}(3) R_{\gamma\delta} \psi_{\gamma}^{\dagger}(2) \psi_{\delta}^{\dagger}(4) |\Omega\rangle, \end{aligned} \quad (17)$$

where R is the charge conjugation matrix define in Eq. 11. These states are linearly independent but are not orthogonal to each other, satisfying $\langle H|V\rangle = \langle V|C\rangle = \langle C|H\rangle = -\frac{1}{4}$. Under the permutation of the four sites $P_{(2341)}$, or a rotation at 90° as shown in Fig. 9 (b), they transform as

$$P_{2341}|H\rangle = |V\rangle, \quad P_{2341}|V\rangle = |H\rangle, \quad P_{2341}|C\rangle = |C\rangle. \quad (18)$$

At $\theta = 45^\circ$, i.e., the $SU(4)_A$ case, the ground state (GS) is exactly an $SU(4)$ singlet over the sites 1 to 4.^{7,36}

$$|\Psi_{SU(4)}^s\rangle = \frac{1}{\sqrt{4!}} \sum_{\mu\nu\tau\xi} \varepsilon_{\mu\nu\tau\xi} \psi_{\mu,1}^{\dagger} \psi_{\nu,2}^{\dagger} \psi_{\tau,3}^{\dagger} \psi_{\xi,4}^{\dagger} |\Omega\rangle, \quad (19)$$

where the indices μ, ν, τ, ξ run over $\pm\frac{3}{2}, \pm\frac{1}{2}$; $|\Omega\rangle$ represents the vacuum state; $\varepsilon_{\mu\nu\tau\xi}$ is a rank-four fully antisymmetric tensor. It can also be represented as the linear combination of the dimer states as

$$|\Psi_{SU(4)}^s\rangle = \sqrt{\frac{2}{3}} (|H\rangle + |V\rangle + |C\rangle), \quad (20)$$

which is even under the rotation operation P_{2341} . We find that in the entire range of $0 \leq \theta < 54^\circ$, the GS

wavefunctions remain even under such a rotation P_{2341} , whose wavefunctions can be represented as

$$|\Psi\rangle = a(|H\rangle + |V\rangle) + b|C\rangle, \quad (21)$$

where a and b are coefficients depending on the values of θ . In fact, the overlaps between GS wavefunctions Eq. 21 and the $SU(4)$ singlet state $|\Psi_{SU(4)}^s\rangle$ are larger than 0.98 at $\theta < 54^\circ$. At $\theta > 54^\circ$, a level crossing occurs and the GS wavefunction changes to

$$|\Psi_{SU(4)}^s\rangle = \sqrt{\frac{2}{3}} (|H\rangle - |V\rangle), \quad (22)$$

which is independent of θ and odd under the rotation P_{2341} .

Combining the above observations, we identify that there are two competing states in the system. The boundary is located at $\theta = 54^\circ$. Next we turn to analyze large size systems.

B. The Low energy spectra for the 4×4 cluster

In this subsection we study a larger system size of $N = 4 \times 4$. Both $L_{15}^{tot} = \sum_i L_{15}(i)$ and $L_{23}^{tot} = \sum_i L_{23}(i)$ are good quantum numbers, which can be used to reduce the Hilbert space. The dimension of the Hilbert space in the $(L_{15}^{tot}, L_{23}^{tot}) = (0, 0)$ sector goes up to 165 million. On the other hand, the lowest multiplet states are located in the sector of $(L_{15}^{tot}, L_{23}^{tot}) = (0, \pm 1)$ or $(\pm 1, 0)$ and the corresponding dimension is about 147 million. The dimensions of the subspace are too large to perform diagonalization. Nevertheless, by using translational symmetry, the dimension of the Hilbert space reduces to 10 million such that ED calculations become doable. The ground states are always in the sector of total momentum $\vec{K} = (0, 0)$, and are $Sp(4)$ singlets. In the following, except for the specific mention in Sec. IV E, the systems are considered under periodic boundary conditions.

The low-lying energy spectra for the $N = 4 \times 4$ clusters for $0 < \theta < 90^\circ$ are displayed in Fig. 10. The ground states for all the values of θ are $Sp(4)$ singlets with Casimir $C = 0$, and that at $\theta = 45^\circ$ is an $SU(4)$ singlet. The lowest excited states are also $Sp(4)$ singlet states at $\theta < 63^\circ$. The lowest spin multiplets appear as the 14-fold degenerate $Sp(4)$ symmetric tensor states with $C = 10$. A level crossing of the lowest excited states appears around $\theta = 63^\circ$ implying that there exists competing phases nearby. At $\theta > 63^\circ$, the lowest excited states become 5-fold degenerate $Sp(4)$ vector states with the Casimir $C = 4$. Another 10-fold degenerate states, which form the $Sp(4)$ adjoint representation with $C = 10$, appear as the next lowest excited states. At the $SU(4)_B$ line, i.e., $\theta = 90^\circ$, these two sectors merge into the 15-fold degenerate states forming the adjoint representation of the $SU(4)$ group whose $SU(4)$ Casimir is $C = 8$.

In Sec. III A, the appearance of the $Sp(4)$ singlet as the lowest excited states in the small size systems implies the dimerization in the thermodynamic limit. This

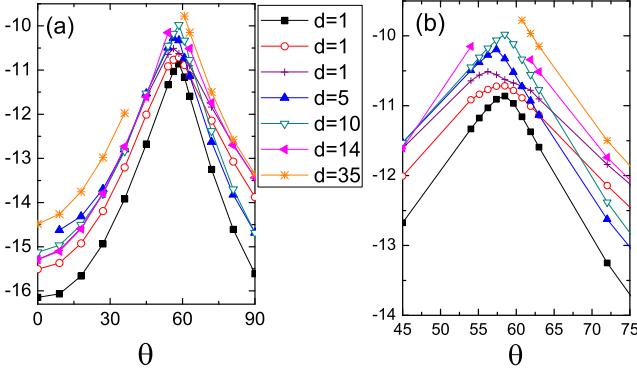


FIG. 10: (a) The low-lying states for the 4×4 cluster at various values of θ . The dimensions of the corresponding $Sp(4)$ representations d are marked. The GS wavefunctions are always $Sp(4)$ singlets. (b) The zooming-in around $\theta \approx 63^\circ$ exhibiting various energy level crossings.

is confirmed in the large size DMRG results in Sec. III B. Similarly, in the case of the 4×4 cluster, the lowest excited states are also $Sp(4)$ singlet at $\theta < 63^\circ$. This also suggests the spin disordered ground state with broken translational symmetry in the thermodynamic limit. Moreover, the gap between the GS and lowest singlet excited state is very small in a narrow regime (roughly $50^\circ \sim 60^\circ$), which implies that an intermediate phase may exist exhibiting a different translational symmetry breaking pattern from that with small values of θ . However, unlike the 1D case where we can justify the dimerization through finite-size scaling of the vanishing of the $Sp(4)$ singlet-singlet gap, it is impossible in 2D to detect the presence of the dimer states or plaquette states from the exact diagonalization results. Thus we will resort to other approaches to investigate the GS profile in the following sections.

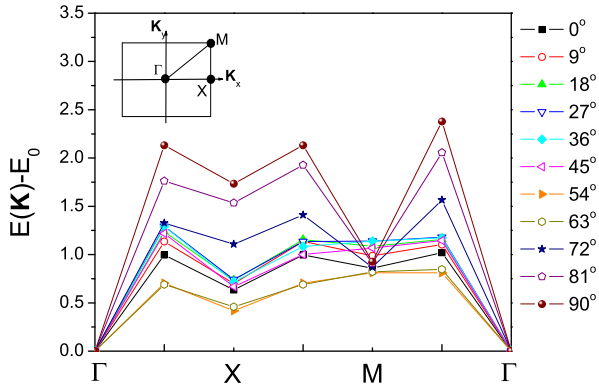


FIG. 11: The energy dispersion $E(\vec{K}) - E_0$ v.s. θ for the 4×4 cluster. Γ , M , X are the high symmetry points for the many-body ground state momenta, corresponding to $\vec{K} = (0, 0)$, (π, π) and $(\pi, 0)$ respectively, in the first Brillouin zone.

To further clarify, in Fig. 11 we present the spectra of lowest energy states at each crystal momentum of

$\Gamma = (0, 0)$, $X = (\pi, 0)$, and $M = (\pi, \pi)$, respectively. At $\theta \leq 63^\circ$, the states at the X -point are lower than those at M -point, which are $Sp(4)$ singlets with the Casimir $C = 0$. These lowest singlet excitations along $(\pi, 0)$ or $(0, \pi)$ would allow the GS to shift a lattice constant along x or y -direction, if the gap between these singlets vanishes in the thermodynamic limit. It would implies a four-fold degeneracy in the thermodynamic limit breaking translational symmetry.

In comparison, as $\theta \geq 72^\circ$, the energy of states at the M -point are lower than those at the X -point, which are spin multiplet with 10-fold degeneracy and the $Sp(4)$ Casimir $C = 6$. Actually, these states are not the lowest excited states which are 5-fold degenerate located at the Γ -point. Nevertheless, their energy splitting from the 10-fold states is very small as shown in Fig. 10. In the thermodynamic limit, inspired by the QMC result of the occurrence of the long-range ordering in the $SU_B(4)$ case, we infer the long-range staggered Neel ordering of the $Sp(4)$ spin operators L_{ab} and a long-range uniform ordering of $Sp(4)$ vector operators n_a . Thus we infer a phase transition from spin disordered ground state to the Neel-like state breaking $Sp(4)$ symmetry.

Let us make an analogy with the 2D spin- $\frac{1}{2}$ J_1 - J_2 model^{51,52}. In that case, the behavior of the low-lying energy levels indicates that the lowest excited states with nonzero momentum are triplet while the system is a magnetic Neel ($J_2/J_1 \lesssim 0.4$) and collinear state ($J_2/J_1 \gtrsim 0.6$), corresponding to $\vec{K} = (\pi, \pi)$ and $(\pi, 0)$, respectively. However, there exists an intermediate phase in $0.4 < J_2/J_1 < 0.6$, where the GS is a magnetic disordered state and the lowest excited state with nonzero momentum, $\vec{K} = (\pi, 0)$, is singlet. In this region it has been conjectured that the GS is a dimerization state or a spin-liquid (resonated-valence-bond state). Similarly, the low-lying energy behavior in our model implies that the GS is non-magnetic at $\theta < 63^\circ$. On the other hand, at $\theta \geq 63^\circ$, the GS has spinful excitations and is relevant to the Neel state.

C. The magnetic structure form factor

In this subsection, we present the results of the magnetic structure form factors for the $N = 4 \times 4$ cluster. Two different structure form factors $S_L(\vec{q})$ and $S_n(\vec{q})$ are defined for the $Sp(4)$ generator and vector channels, respectively, as

$$S_L(\vec{q}) = \frac{1}{g_L N^2} \sum_{i,j, 1 \leq a < b \leq 5} e^{i\vec{q} \cdot (\vec{r}_i - \vec{r}_j)} \langle G | L_{ab}(i) L_{ab}(j) | G \rangle,$$

$$S_n(\vec{q}) = \frac{1}{g_n N^2} \sum_{i,j, a=1 \sim 5} e^{i\vec{q} \cdot (\vec{r}_i - \vec{r}_j)} \langle G | n_a(i) n_a(j) | G \rangle, \quad (23)$$

where the normalization constants $g_L = 10$ and $g_n = 5$. $S_L(\vec{q})$ and $S_n(\vec{q})$ are the analogy of the Fourier transformation of $\langle G | \vec{S}_i \cdot \vec{S}_j | G \rangle$ in $SU(2)$ systems. If the long-range magnetic order appears, the magnetic structure

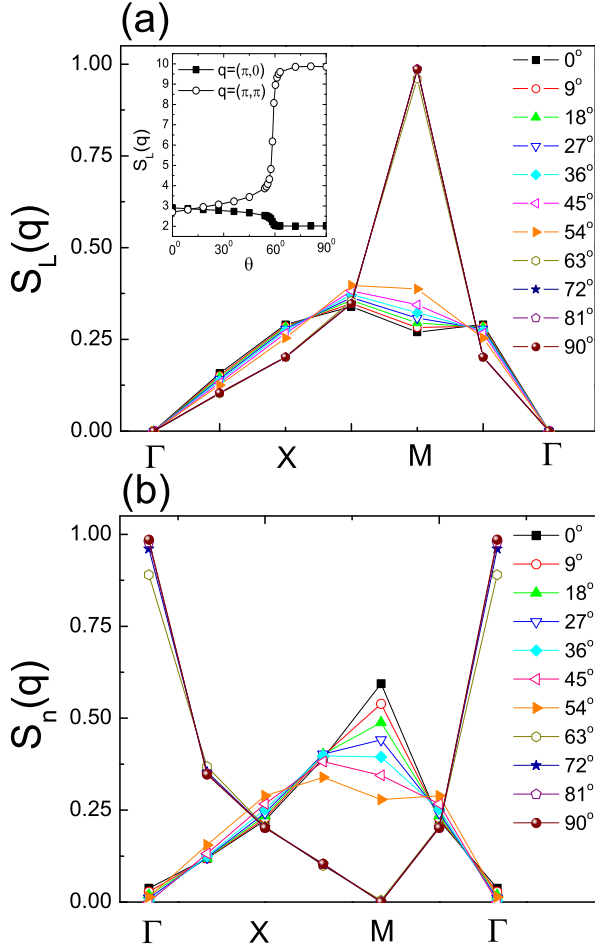


FIG. 12: The magnetic structure factors for the 4×4 cluster. (a) The structure factors $S_L(\vec{q})$ for the $Sp(4)$ generator sector. The inset is the comparison between $S_L(\pi, 0)$ and $S_L(\pi, \pi)$ versus θ . (b) The $Sp(4)$ vector structure factor $S_n(\vec{q})$.

factor converges to a finite value in the thermodynamic limit^{40,53}.

The ED results of $S_L(\vec{q})$ for the 4×4 cluster are presented in Fig. 12 (a). As $\theta \lesssim 60^\circ$, $S_L(\vec{q})$ distributes smoothly over all the momenta, and its maximum is located at $\vec{q} = (\pi, \frac{\pi}{2})$, which is slightly larger than other values of \vec{q} . In contrast, when $60^\circ \lesssim \theta \leq 90^\circ$, $S_L(\vec{q})$ peaks at $\vec{K}_M = (\pi, \pi)$. The $Sp(4)$ vector channel structure factor $S_n(\vec{q})$ is depicted in Fig. 12 (b). At small values of θ , it peaks at the M-point exhibiting a dominate correlation at the momentum (π, π) . As $\theta \gtrsim 60^\circ$, the peak changes to the Γ point and the M-point becomes a minimum.

Along the $SU(4)_B$ line with $\theta = 90^\circ$, $S_n(\vec{q}) = S_L(\vec{q} + \vec{K}_M)$ due to the staggered definition of $Sp(4)$ vectors n_a in Eq. 12. This relation between $S_n(\vec{q})$ and $S_L(\vec{q} + \vec{K}_M)$ is consistent with the previous observation on the low-energy spectra in Fig. 10. As $\theta \geq 60^\circ$ there are two nearly degenerate excited states beyond the GS, having the total momentum of $(0, 0)$ and (π, π) . They correspond to the 5d vector representation with $C = 4$ and the

10d tensor representation with $C = 6$ in the $Sp(4)$ symmetry, respectively. The contributions to $S_n(\vec{K}_\Gamma)$ and $S_L(\vec{K}_M)$ mainly come from the matrix elements between the ground state and the 5d vector states, and 10d anti-symmetric tensor states, respectively. On the other hand, in the case of $SU(4)_A$ with $\theta = 45^\circ$, $S_n(\vec{q}) = S_L(\vec{q})$ for each \vec{q} .

These features highlight that the dominant Neel correlation of the $Sp(4)$ generators L_{ab} 's not only exhibits along the $SU(4)_B$ line but also extends to a finite regime with non-zero values of J_2 . In the same parameter regime, the $Sp(4)$ vectors n_a 's exhibit dominant uniform correlations. The critical value of θ of the onset of the outstanding $S_L(\pi, \pi)$ is in good agreement with the location of the level crossing shown in Fig. 10, implying a transition of the GS from a non-Neel state to a Neel type. The inset in Fig. 12 (a) compares the $S_L(\vec{q})$ behavior at $\vec{q} = (\pi, 0)$ and (π, π) versus θ . $S_L(\pi, 0)$ changes little as varying θ . Therefore, it is inferred that only the Neel-type order exists at θ close to 90° . The magnetic ordering at $(\pi, 0)$ should not appear in the 2D $Sp(4)$ system.

Next one may raise a natural question: what is the spin pattern for the Neel-order state as $\theta \rightarrow 90^\circ$? According to Eq. 12, its classic energy can be minimized by choosing a staggered configuration for $\langle G | L_{15}(i) | G \rangle = \langle G | L_{23}(i) | G \rangle = (-)^i \frac{1}{2}$ and a uniform configuration of $\langle G | n_4(i) | G \rangle = \pm \frac{1}{2}$. These correspond to the staggered arrangement in the 2D lattice by using the two components of $F_z = \pm \frac{3}{2}$, or by using the other two components of $F_z = \pm \frac{1}{2}$. These different classic Neel states can be connected by an $Sp(4)$ rotation.

D. The columnar dimer correlations

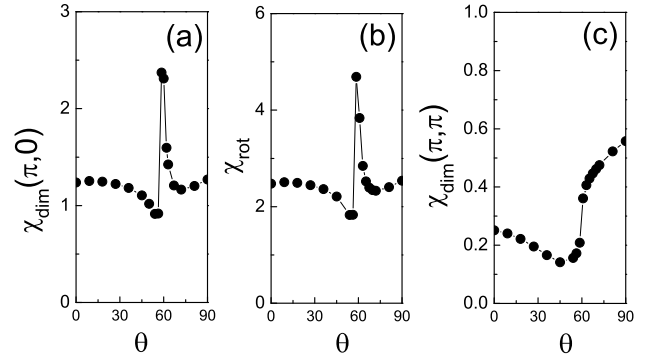


FIG. 13: The susceptibilities defined in Eq. 24 with respect to the perturbations O_{dim} and O_{rot} for the $N = 4 \times 4$ cluster. (a) $\chi_{dim}(\vec{Q})$ versus θ at $\vec{Q} = (\pi, 0)$; (b) χ_{rot} versus θ ; (c) $\chi_{dim}(\vec{Q})$ versus θ at $\vec{Q} = (\pi, \pi)$. In both cases, a small value of $\delta = 0.01$ is taken to evaluate the susceptibilities. Both susceptibilities exhibit peaks around $\theta \approx 60^\circ \sim 70^\circ$.

In this subsection, we discuss the possibility of the dimer-ordered state at intermediate values of θ . We de-

fine the susceptibility to a symmetry breaking perturbation as

$$\chi(\delta) = -\frac{2[e(\delta) - e(0)]}{\delta^2}, \quad (24)$$

where $e(0)$ is the GS energy per site given by the Hamiltonian Eq. (7) and $e(\delta)$ is Eq. 7 plus the corresponding perturbation term $-\delta\hat{O}^{54,55}$. In the presence of long-range ordering, the corresponding susceptibility $\chi = \lim_{\delta \rightarrow 0} \chi(\delta)$ will diverge in the thermodynamic limit. It has been demonstrated that this approach can efficiently distinguish dimerized and non-dimerized phases in the 1D J_1 - J_2 spin- $\frac{1}{2}$ chain⁵⁵, in which the phase boundary $J_2/J_1 \approx 0.24$ between these two phases.

Here we employ the same method to study the dimerization correlations. Although with small size calculations, we are unable to determine the existence of long range order, it is still instructive to observe the feature of χ . We have used it to test the 1D $Sp(4)$ system with the perturbation term of $\hat{O} = \sum_i (-1)^i H_{ex}(i, i+1)$. At $\theta = 60^\circ$, we found the dramatic growing behavior of $\chi(\delta)$ upon decreasing δ and increasing the system size, which leads to a divergent χ in the thermodynamic limit. On the other hand, $\chi(\delta)$ at $\theta = 30^\circ$ has no tendency of divergence over decreasing δ . This observation is consistent with our previous analytical and numerical studies: the 1D $Sp(4)$ system is either a gapless uniform liquid as $\theta \leq 45^\circ$ or a gapped dimerized state with the breaking of translation symmetry at $\theta > 45^\circ$.

Next we apply this method to the 2D system with the size of 4×4 , and define two susceptibilities $\chi_{dim}(\vec{Q})$ and χ_{rot} for two perturbations of $\hat{O}_{dim}(\vec{Q})$ and \hat{O}_{rot} as

$$\hat{O}_{dim}(\vec{Q}) = \sum_i \cos(\vec{Q} \cdot \vec{r}_i) H_{ex}(i, i + \hat{x}), \quad (25)$$

$$\hat{O}_{rot} = \sum_i [H_{ex}(i, i + \hat{x}) - H_{ex}(i, i + \hat{y})], \quad (26)$$

where $H_{ex}(i, j)$ is defined as one bond of the Hamiltonian Eq. 7 without summation over i and j . Let us set $\vec{Q} = (\pi, 0)$, thus $\chi_{dim}(\pi, 0)$ corresponds to the instability to the columnar dimer configuration. Eq. 25 and Eq. 26 break the translational symmetry along the x -direction and rotational symmetry, respectively. The plaquette ordering maintains the 4-fold rotational symmetry, thus will lead to the divergence of $\chi_{dim}(\pi, 0)$ but not χ_{rot} . The ED results for the susceptibilities with respect to the two perturbations versus θ in Fig. 13 (a) and (b), respectively. A small value of $\delta = 0.01$ is taken. Both susceptibilities exhibit a peak at θ from 60° to 70° , which implies a tendency to breaking both translational and rotational symmetries. This shows that the columnar dimerization instead of the plaquette ordering is a promising instability in this regime in the thermodynamic limit. We have also calculated the susceptibility of $\chi_{dim}(\vec{Q})$ for $\vec{Q} = (\pi, \pi)$ which corresponds to the instability to the staggered dimer configuration in Fig. 13

(c). Although the magnitudes of $\chi_{dim}(\pi, \pi)$ are smaller than $\chi_{dim}(\pi, 0)$ and χ_{rot} , it suddenly raises up around $\theta = 60^\circ$.

E. The plaquette form factor

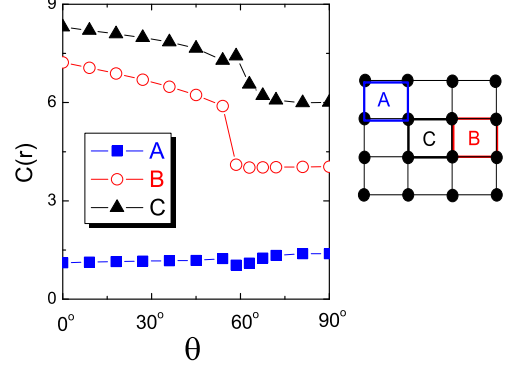


FIG. 14: $C(\vec{r})$ defined in Eq. 27 versus θ . The positions of plaquette A, B and C are defined on the right schematics. A (blue) is located at the corner whereas C (black) in the most middle one.

In this subsection, we consider the plaquette type correlation. The ground states of the 4×4 cluster at $\theta \lesssim 60^\circ$ signal a different class from that in $\theta \geq 63^\circ$ in which the lowest excited states are spin multiplet with $\vec{K} = (\pi, \pi)$. Here, the lowest excited states remain $Sp(4)$ singlets with $\vec{K} = (\pi, 0)$ or $(0, \pi)$. To further elucidate the ground state profile, we define the local Casimir for the plaquette centered at \vec{r} ,

$$C(\vec{r}) = \langle G | \sum_{1 \leq a < b \leq 5} \left\{ \sum_i L_{ab}(i) \right\}^2 | G \rangle, \quad (27)$$

where i runs over the four sites of this plaquette. The $SU(2)$ version of Eq. 27 has been used to classify competing dimer and plaquette orders⁵⁶. If the GS exhibits a strong plaquette pattern, for instance, indicated as phase A in Fig. 8, the magnitudes of $C(\vec{r})$ will have obvious spatial variations between nearest-neighboring plaquette. This is analogous to the 1D dimerization picture in Fig. 5 (a), where the nearest-neighboring spin-spin correlations exhibit strong and weak alternately in magnitude. When the spins around a plaquette are strongly bound to form an $SU(4)$ singlet, $C(\vec{r})$ should be close to zero.

Fig. 14 depicts the behavior of $C(\vec{r})$ at various values of θ for the 4×4 cluster. In order to explicitly reflect the plaquette formation, we use *open* boundary conditions rather than periodic boundary conditions. In this case only C_{4v} point group symmetry is applicable in the ED. The $C(\vec{r})$ for the corner plaquette A is much smaller than $\frac{1}{5}$ of those at the center C and the middle of the edge B for small values of θ . This is in sharp contrast to the 2D spin-1/2 model which renders $C(A) = 0.545$, $C(B) = 1.015$ and $C(C) = 1.282$, which only show the difference

at order of 1. The comparison suggests the pinning-down plaquette state in the 2D $Sp(4)$ system under the open boundary. We observe that $C(A)$ and $C(B)$ decrease while θ goes beyond 60° . It accounts for the formation of the plaquette-type pattern weakens or even vanishes.

Combined the above observations, it is likely that for $\theta < 60^\circ$ the GS has a strong plaquette-like correlation, that could be the resonate plaquette state proposed by Bossche *et al.*³⁷ or a certain spin-liquid. It does survive not only along the $SU(4)_A$ line but also in a finite regime. Nevertheless, we have to emphasize that this picture cannot be conclusively determined due to finite size effects and further larger size calculations are needed to confirm.

V. CONCLUSION

In conclusion, we study an $Sp(4)/SO(5)$ spin Heisenberg model which can be realized by the large spin ultra-cold fermions with $F = \frac{3}{2}$. The $Sp(4)$ Heisenberg model describing the magnetic exchange at the insulating state of quarter-filling is simulated by exact diagonalization and DMRG. In 1D, our numerical results are in agreement with previous analytic studies. There are two competing phases: a gapped dimer phase with spin gap at $\theta > 45^\circ$ and a gapless spin liquid at $\theta \leq 45^\circ$. The phase boundary is identified as $\theta = 45^\circ$ which belongs to $SU(4)_A$ -type symmetry. In the gapless spin liquid phase, the static correlation functions decay algebraically with four-site periodicity oscillations.

We also investigate the $Sp(4)$ spin model on a 2D square lattice up to 16 sites by means of exact diagonalization methods. Our numerical results show three competing correlations: Neel-type, plaquette formation and columnar spin-Peierls dimerization, depending on θ 's. Such observation can have phase behavior analogy in comparison with the speculated phase diagram depicted in Fig. 8. Due to the finite size effects, however, we are unable to conclusively identify the existence of these phases and the phase boundaries based on the small cluster. More numerical studies are necessary to further explore the phase diagram in the thermodynamic limit.

Acknowledgments

H. H. H. is grateful to helpful discussions with Stephan Rachel and computational facilities from Tunghai University. H. H. H. also appreciates Zi Cai and Cheng-Chien Chen for fruitful discussions and suggestions on exact diagonalization techniques. H. H. H. and C. W. are supported by NSF under No. DMR-0804775. Y. P. W. is supported by NSFC and 973-project of MOST China.

Appendix A: Representation theory of the simple Lie groups and algebras

The representation theory of Lie groups and algebras can be found in standard group theory textbooks⁵⁷. Here we give a brief pedagogical introduction. Among the group generators, we choose the maximal set of generators that commute with each other as the *Cartan sub-algebra* $\{H_i, (i = 1, \dots, k)\}$, where k is called the rank of the Lie algebra. For example, the $SU(2)$ algebra is rank one, whose Cartan sub-algebra only contains S_z . All other generators can be organized as eigen-operators of each generator in the Cartan sub-algebra, which are called *roots*. Roots always appear in terms of Hermitian conjugate pairs as $E_{j\pm}$ with the relation $E_{j-} = E_{j+}^\dagger$. They satisfy the commutation relations of

$$[H_i, E_{\pm j}] = \alpha_{\pm j}(i) E_{\pm j}, \quad (A1)$$

with $\vec{\alpha}_j = -\vec{\alpha}_{-j}$, where the i -th elements of the vectors $\vec{\alpha}_{\pm j}$ are the eigenvalue of $E_{\pm j}$ with respect to H_i . For example, for the simplest $SU(2)$ case, the roots are $S_\pm = S_x \pm iS_y$ and $[S_z, S_\pm] = \pm S_\pm$, where α_\pm only have one component with $\alpha_\pm = \pm 1$.

Among all the roots, we fix the convention to use E_{+j} for *positive roots*, which means the first non-zero components of their $\vec{\alpha}_{+j}$ are positive. Positive roots can be decomposed into the linear combinations of *simple roots* with non-negative integer coefficients. The number of simple roots of a simple Lie algebra equals to its rank. The *Cartan matrix* A of a simple Lie algebra is defined as

$$A_{ij} = 2 \frac{(\vec{\alpha}_i, \vec{\alpha}_j)}{(\vec{\alpha}_i, \vec{\alpha}_i)}, \quad (i, j = 1, \dots, k), \quad (A2)$$

where $\vec{\alpha}_i$ is the vector of eigenvalues of the simple root E_i ; the inner products of α -vectors is defined as

$$(\vec{\alpha}_i, \vec{\alpha}_j) = \sum_{l=1}^k \alpha_i(l) \alpha_j(l). \quad (A3)$$

The dimension of the Cartan matrix is the same as the Cartan sub-algebra. For the $SU(2)$ group, the only positive and simple root is S_+ , and the 1×1 Cartan matrix $A = 2$.

An important concept of the representations of the simple Lie algebra is *weight*. For a rank- k simple Lie algebra, its fundamental weights can be solved through its $k \times k$ Cartan matrix

$$\vec{M}_i = \sum_j \vec{\alpha}_j (A^{-1})_{ji}, \quad (i = 1, \dots, k). \quad (A4)$$

Any irreducible representation of a simple Lie algebra is uniquely determined by its highest weight \vec{M}^* , which can be written as a linear combination of the fundamental weights \vec{M}_i

$$\vec{M}^* = \sum_i \mu_i \vec{M}_i, \quad (i = 1, \dots, k), \quad (A5)$$

where μ 's are non-negative integers. The dimension of the representation M^* is

$$d(M^*) = \prod_{\text{positive roots}} \left[1 + \frac{(\vec{M}^*, \vec{\alpha}_i)}{(\vec{R}, \vec{\alpha}_i)} \right], \quad (\text{A6})$$

with

$$\vec{R} = \frac{1}{2} \sum_{\text{positive roots}} \vec{\alpha}_i. \quad (\text{A7})$$

Please notice that the product in Eq. A6 and summation in Eq. A7 take over all the positive roots. The value of the *Casimir* operator for the representation denoted by M^* is

$$C(\vec{M}^*) = (\vec{M}^*, \vec{M}^* + 2\vec{R}). \quad (\text{A8})$$

For the simplest example of $SU(2)$, the only fundamental weight $M = \frac{1}{2}$. The highest weights is just $M^* = S$, where S takes half-integer and integer numbers. Obviously, $d(S) = 2S + 1$ and $C(S) = S(S + 1)$ as expected.

Appendix B: The $Sp(4)(SO(5))$ algebra

For convenience, we use the following symbols to represent the $Sp(4)(SO(5))$ generators L_{ab} ($1 \leq a < b \leq 5$) defined in Eq. 5 as

$$L_{ab} = \begin{pmatrix} 0 & \text{Re}\pi_x & \text{Re}\pi_y & \text{Re}\pi_z & Q \\ & 0 & -S_z & S_y & \text{Im}\pi_x \\ & & 0 & -S_x & \text{Im}\pi_y \\ & & & 0 & \text{Im}\pi_z \\ & & & & 0 \end{pmatrix}, \quad (\text{B1})$$

where

$$\begin{aligned} \pi_x^\dagger &= \text{Re}\pi_x + i\text{Im}\pi_x = \psi_{\frac{3}{2}}^\dagger \psi_{-\frac{3}{2}} + \psi_{\frac{1}{2}}^\dagger \psi_{-\frac{1}{2}}, \\ \pi_x &= \text{Re}\pi_x - i\text{Im}\pi_x = \psi_{\frac{3}{2}}^\dagger \psi_{\frac{3}{2}} + \psi_{-\frac{1}{2}}^\dagger \psi_{\frac{1}{2}}, \\ \pi_y^\dagger &= \text{Re}\pi_y + i\text{Im}\pi_y = -i(\psi_{\frac{3}{2}}^\dagger \psi_{-\frac{3}{2}} - \psi_{\frac{1}{2}}^\dagger \psi_{-\frac{1}{2}}), \\ \pi_y &= \text{Re}\pi_y - i\text{Im}\pi_y = i(\psi_{\frac{3}{2}}^\dagger \psi_{\frac{3}{2}} - \psi_{-\frac{1}{2}}^\dagger \psi_{\frac{1}{2}}), \\ \pi_z^\dagger &= \text{Re}\pi_z + i\text{Im}\pi_z = \psi_{\frac{3}{2}}^\dagger \psi_{-\frac{1}{2}} - \psi_{\frac{1}{2}}^\dagger \psi_{-\frac{3}{2}}, \\ \pi_z &= \text{Re}\pi_z - i\text{Im}\pi_z = \psi_{-\frac{1}{2}}^\dagger \psi_{\frac{3}{2}} - \psi_{-\frac{3}{2}}^\dagger \psi_{\frac{1}{2}}, \\ S_+ &= S_x + iS_y = \psi_{\frac{3}{2}}^\dagger \psi_{\frac{1}{2}} - \psi_{-\frac{1}{2}}^\dagger \psi_{-\frac{3}{2}}, \\ S_- &= S_x - iS_y = \psi_{\frac{1}{2}}^\dagger \psi_{\frac{3}{2}} - \psi_{-\frac{3}{2}}^\dagger \psi_{-\frac{1}{2}}, \\ S_z &= \frac{1}{2}(\psi_{\frac{3}{2}}^\dagger \psi_{\frac{3}{2}} - \psi_{\frac{1}{2}}^\dagger \psi_{\frac{1}{2}} + \psi_{-\frac{1}{2}}^\dagger \psi_{-\frac{1}{2}} - \psi_{-\frac{3}{2}}^\dagger \psi_{-\frac{3}{2}}), \\ Q &= \frac{1}{2}(\psi_{\frac{3}{2}}^\dagger \psi_{\frac{3}{2}} + \psi_{\frac{1}{2}}^\dagger \psi_{\frac{1}{2}} - \psi_{-\frac{1}{2}}^\dagger \psi_{-\frac{1}{2}} - \psi_{-\frac{3}{2}}^\dagger \psi_{-\frac{3}{2}}). \end{aligned} \quad (\text{B2})$$

(Q, S_z)	Roots
$\alpha_{\pm 1} = \pm(1, -1)$	$E_1 = \frac{1}{\sqrt{24}}(\pi_x^\dagger - i\pi_y^\dagger); E_{-1} = \frac{1}{\sqrt{24}}(\pi_x + i\pi_y)$
$\alpha_{\pm 2} = \pm(0, 1)$	$E_2 = \frac{1}{\sqrt{12}}(S_x + iS_y); E_{-2} = \frac{1}{\sqrt{12}}(S_x - iS_y)$
$\alpha_{\pm 3} = \pm(1, 1)$	$E_3 = \frac{1}{\sqrt{24}}(\pi_x^\dagger + i\pi_y^\dagger); E_{-3} = \frac{1}{\sqrt{24}}(\pi_x - i\pi_y)$
$\alpha_{\pm 4} = \pm(1, 0)$	$E_4 = \frac{1}{\sqrt{12}}\pi_z^\dagger; E_{-4} = \frac{1}{\sqrt{12}}\pi_z$

TABLE I: Cartan sub-algebra and its roots. $[E_1, E_{-1}] = \frac{1}{6}(Q - S_z)$, $[E_2, E_{-2}] = \frac{1}{6}S_z$, $[E_3, E_{-3}] = \frac{1}{6}(Q + S_z)$, $[E_4, E_{-4}] = \frac{1}{6}Q$.

	(μ_1, μ_2)	M^*	$d(M^*)$	$C(\vec{M}^*)$
1	(0,0)	(0,0)	1	0
2	(0,1)	$(\frac{1}{2}, \frac{1}{2})$	4	$\frac{5}{2}$
3	(1,0)	(1,0)	5	4
4	(0,2)	(1,1)	10	6
5	(2,0)	(2,0)	14	10
6	(1,1)	$(\frac{3}{2}, \frac{1}{2})$	16	$\frac{15}{2}$
7	(1,2)	(2,1)	35	12
8	(0,3)	$(\frac{3}{2}, \frac{3}{2})$	20	$\frac{21}{2}$

TABLE II: Some irreducible representations of the $Sp(4)/SO(5)$ group: the highest weights, dimensions and Casimirs.

The ten operators of $Sp(4)$ satisfy the commutation relations

$$[L_{ab}, L_{cd}] = -i(\delta_{bc}L_{ad} + \delta_{ad}L_{bc} - \delta_{ac}L_{bd} - \delta_{bd}L_{ac}), \quad (\text{B3})$$

which is rank-2 Lie algebra. Its Cartan sub-algebra only contains two commutable generators H_i ($i = 1, 2$), which can be chosen as ($H_1 = S_z, H_2 = Q$). We group the other 8 generators as their eigen-operators, *i.e.*, roots as represented $E_{\pm 1}, E_{\pm 2}, E_{\pm 3}, E_{\pm 4}$, whose eigenvalue vectors $\vec{\alpha}_{\pm j}$ are presented in Tab. I. The simple roots are E_1 with $\vec{\alpha}_1 = (1, -1)$ and E_2 with $\vec{\alpha}_2 = (0, 1)$. The other roots can be represented as $E_3 = E_1 + 2E_2, E_4 = E_1 + E_2$. The $Sp(4)/SO(5)$ Cartan matrix reads

$$A = \begin{pmatrix} 2 & -1 \\ -2 & 2 \end{pmatrix}. \quad (\text{B4})$$

We solve the fundamental weights as $\vec{M}_1 = (1, 0), \vec{M}_2 = (\frac{1}{2}, \frac{1}{2})$ from Eq. A4. The highest weight \vec{M}^* can be written as

$$\vec{M}^* = (m_1, m_2) = (\mu_1 + \frac{\mu_2}{2}, \frac{\mu_2}{2}), \quad (\text{B5})$$

where $\mu_{1,2}$ are non-negative integers. The dimension of the corresponding representation is

$$\begin{aligned} d(\mu_1, \mu_2) &= (1 + \mu_1)(1 + \mu_2)(1 + \frac{2\mu_1 + \mu_2}{3}) \\ &\times (1 + \frac{\mu_1 + \mu_2}{2}). \end{aligned} \quad (\text{B6})$$

The representation (μ_1, μ_2) belongs to the category of tensor or spinor representations of $Sp(4)$ when μ_2 is even or odd, respectively. The Casimir operator reads

$$\begin{aligned} C(\vec{M}^*) &= \sum_{a < b} L_{ab}^2 = Q^2 + S_z^2 + 6 \sum_{\alpha} \{E_{\alpha}, E_{-\alpha}\} \\ &= m_1(m_1 + 3) + m_2(m_2 + 1). \end{aligned} \quad (B7)$$

We summarize some frequently used representations of $Sp(4)(SO(5))$ in Table II. The representations with indices 1 to 5 are particularly useful. They are the identity (1d), the fundamental spinor (4d), vector (5d), adjoint (10d), symmetric traceless tensor (14d) representations of the $SO(5)$ group, respectively.

Appendix C: $SU(4)(SO(6))$ algebra

The $SU(4)$ group is isomorphic to $SO(6)$. Their relation is similar to that between $SU(2)$ and $SO(3)$, or $Sp(4)$ and $SO(5)$. As represented in Eq. 5, L_{ab} and the five spin-quadrupole operators $n_a = \psi_{\alpha}^{\dagger} \Gamma_{\alpha\beta}^a \psi_{\beta}$ together form the 15 generators of the $SU(4)$ group. Explicitly, the generators of n_a s are written as

$$\begin{aligned} n_1 &= \frac{i}{2}(\psi_{\frac{3}{2}}^{\dagger} \psi_{-\frac{1}{2}} + \psi_{\frac{1}{2}}^{\dagger} \psi_{-\frac{3}{2}} - \psi_{-\frac{1}{2}}^{\dagger} \psi_{\frac{3}{2}} - \psi_{-\frac{3}{2}}^{\dagger} \psi_{\frac{1}{2}}), \\ n_2 &= \frac{1}{2}(\psi_{\frac{3}{2}}^{\dagger} \psi_{\frac{1}{2}} + \psi_{\frac{1}{2}}^{\dagger} \psi_{\frac{3}{2}} - \psi_{-\frac{1}{2}}^{\dagger} \psi_{-\frac{3}{2}} - \psi_{-\frac{3}{2}}^{\dagger} \psi_{-\frac{1}{2}}) \\ n_3 &= -\frac{i}{2}(\psi_{\frac{3}{2}}^{\dagger} \psi_{\frac{1}{2}} - \psi_{\frac{1}{2}}^{\dagger} \psi_{\frac{3}{2}} - \psi_{-\frac{1}{2}}^{\dagger} \psi_{-\frac{3}{2}} + \psi_{-\frac{3}{2}}^{\dagger} \psi_{-\frac{1}{2}}) \\ n_4 &= \frac{1}{2}(\psi_{\frac{3}{2}}^{\dagger} \psi_{\frac{3}{2}} - \psi_{\frac{1}{2}}^{\dagger} \psi_{\frac{1}{2}} - \psi_{-\frac{1}{2}}^{\dagger} \psi_{-\frac{1}{2}} + \psi_{-\frac{3}{2}}^{\dagger} \psi_{-\frac{3}{2}}) \\ n_5 &= -\frac{1}{2}(\psi_{\frac{3}{2}}^{\dagger} \psi_{-\frac{1}{2}} + \psi_{\frac{1}{2}}^{\dagger} \psi_{-\frac{3}{2}} + \psi_{-\frac{1}{2}}^{\dagger} \psi_{\frac{3}{2}} + \psi_{-\frac{3}{2}}^{\dagger} \psi_{\frac{1}{2}}). \end{aligned} \quad (C1)$$

The rank of the $SU(4)$ group is three. We choose (Q, S_z, n_4) as Cartan sub-algebra and group the other 12 generators as roots as shown in Tab. III.

(Q, S_z, n_4)	roots
$\alpha_{\pm 1} = \pm(1, -1, 0)$	$F_1 = \frac{1}{\sqrt{32}}(\pi_x^{\dagger} - i\pi_y^{\dagger}) = \frac{1}{\sqrt{8}}\psi_{\frac{1}{2}}^{\dagger}\psi_{-\frac{1}{2}}$
$\alpha_{\pm 2} = \pm(0, 1, -1)$	$F_2 = \frac{(S_x + iS_y) - (n_2 + in_3)}{\sqrt{32}} = \frac{1}{\sqrt{8}}\psi_{-\frac{1}{2}}^{\dagger}\psi_{-\frac{3}{2}}$
$\alpha_{\pm 3} = \pm(0, 1, 1)$	$F_3 = \frac{1}{\sqrt{32}}(S_x + iS_y + n_2 + in_3) = \frac{1}{\sqrt{8}}\psi_{\frac{3}{2}}^{\dagger}\psi_{\frac{1}{2}}$
$\alpha_{\pm 4} = \pm(1, 1, 0)$	$F_4 = \frac{1}{\sqrt{32}}(\pi_x^{\dagger} + i\pi_y^{\dagger}) = \frac{1}{\sqrt{8}}\psi_{\frac{3}{2}}^{\dagger}\psi_{-\frac{3}{2}}$
$\alpha_{\pm 5} = \pm(1, 0, 1)$	$F_5 = \frac{1}{\sqrt{32}}(\pi_z^{\dagger} - i(n_1 - in_5)) = \frac{1}{\sqrt{8}}\psi_{\frac{3}{2}}^{\dagger}\psi_{-\frac{1}{2}}$
$\alpha_{\pm 6} = \pm(1, 0, -1)$	$F_6 = \frac{1}{\sqrt{32}}(\pi_z^{\dagger} + i(n_1 - in_5)) = \frac{1}{\sqrt{8}}\psi_{\frac{1}{2}}^{\dagger}\psi_{-\frac{3}{2}}$

TABLE III: Cartan sub-algebra and its roots. $[F_1, F_{-1}] = \frac{1}{8}(Q - S_z)$, $[F_2, F_{-2}] = \frac{1}{8}(S_z - n_4)$, $[F_3, F_{-3}] = \frac{1}{8}(S_z + n_4)$, $[F_4, F_{-4}] = \frac{1}{8}(Q + S_z)$, $[F_5, F_{-5}] = \frac{1}{8}(Q + n_4)$, $[F_6, F_{-6}] = \frac{1}{8}(Q - n_4)$.

The simple roots are F_1, F_2 and F_3 with the eigenvalue vectors $\vec{\alpha}_1 = (1, -1, 0)$, $\vec{\alpha}_2 = (0, 1, -1)$, $\vec{\alpha}_3 = (0, 1, 1)$,

respectively. The other positive roots are represented as $F_4 = F_1 + F_2 + F_3$, $F_5 = F_1 + F_3$ and $F_6 = F_1 + F_2$. The $SU(4)/SO(6)$ Cartan matrix reads

$$A = \begin{pmatrix} 2 & -1 & -1 \\ -1 & 2 & 0 \\ -1 & 0 & 2 \end{pmatrix}. \quad (C2)$$

The fundamental weights can be solved by using Eq. A4 as

$$\vec{M}_1 = (1, 0, 0), \vec{M}_2 = (\frac{1}{2}, \frac{1}{2}, -\frac{1}{2}), \vec{M}_3 = (\frac{1}{2}, \frac{1}{2}, \frac{1}{2}). \quad (C3)$$

The highest weight \vec{M}^* of each representation can be chosen as

$$\begin{aligned} \vec{M}^* &= (m_1, m_2, m_3) = \mu_1 \vec{M}_1 + \mu_2 \vec{M}_2 + \mu_3 \vec{M}_3 \\ &= (\mu_1 + \frac{\mu_2}{2} + \frac{\mu_3}{2}, \frac{\mu_2}{2} + \frac{\mu_3}{2}, -\frac{\mu_2}{2} + \frac{\mu_3}{2}). \end{aligned} \quad (C4)$$

The dimension and Casimir of the representation \vec{M}^* are represented as

$$\begin{aligned} d(\vec{M}^*) &= (1 + \mu_1)(1 + \mu_1)(1 + \mu_1)(1 + \frac{\mu_1 + \mu_2}{2}) \\ &\quad \times (1 + \frac{\mu_1 + \mu_3}{2})(1 + \frac{\mu_1 + \mu_2 + \mu_3}{3}), \end{aligned} \quad (C5)$$

$$\begin{aligned} C(\vec{M}^*) &= H_1^2 + H_2^2 + H_3^2 + 8 \sum_{\Delta^+} \{F_{\alpha}, F_{-\alpha}\} \\ &= m_1(m_1 + 4) + m_2(m_2 + 2) + m_3^2. \end{aligned} \quad (C6)$$

Rep	(μ_1, μ_2, μ_3)	$M^*(m_1, m_2, m_3)$	$d(M^*)$	Casimir
1	(0,0,0)	(0,0,0)	1	0
2	(0,0,1)	$(\frac{1}{2}, \frac{1}{2}, \frac{1}{2})$	4	$\frac{15}{4}$
3	(0,1,0)	$(\frac{1}{2}, \frac{1}{2}, -\frac{1}{2})$	4	$\frac{15}{4}$
4	(1,0,0)	(1,0,0)	6	5
5	(0,0,2)	(1,1,1)	10	9
6	(0,2,0)	(1,1,-1)	10	9
7	(0,1,1)	(1,1,0)	15	8
8	(2,0,0)	(2,0,0)	20	12

TABLE IV: Some frequently used irreducible representations of the $SO(6)$ or $SU(4)$ group: the highest weight, dimension and Casimir.

We summarize some frequently used representations of $SU(4)(SO(6))$ in Tab. IV. Representations with indices from 1 to 6 are the identity (1d), the fundamental spinor (4d) and its complex conjugation (4d), the rank-2 anti-symmetric tensor (6d), the rank-2 symmetric tensor (10d) and its complex conjugation (10d), the adjoint (15d) representations, respectively. On the other hand, the Young pattern is often convenient for the representations of $SU(N)$ group. The Young patterns of the representations from 1 to 8 in Tab. IV are shown in Fig. 15.

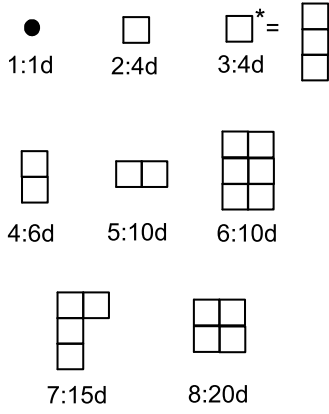


FIG. 15: The Young patterns of the $SU(4)$ representations 1 to 8 presented in Tab. IV.

-
- ¹ B. J. DeSalvo, M. Yan, P. G. Mickelson, Y. N. M. de Escobar, and T. C. Killian, Phys. Rev. Lett. **105**, 030402 (2010).
- ² S. Taie, Y. Takasu, S. Sugawa, R. Yamazaki, T. Tsujimoto, R. Murakami, and Y. Takahashi, Phys. Rev. Lett. **105**, 190401 (2010).
- ³ C. Wu, Physics **3**, 92 (2010).
- ⁴ C. Wu, Mod. Phys. Lett. B **20**, 1707 (2006).
- ⁵ S. K. Yip and T. L. Ho, Phys. Rev. A **59**, 4653 (1999).
- ⁶ T. L. Ho and S. Yip, Phys. Rev. Lett. **82**, 247 (1999).
- ⁷ S. Chen, C. Wu, Y. P. Wang, and S. C. Zhang, Phys. Rev. B **72**, 214428 (2005).
- ⁸ C. Xu and C. Wu, Phys. Rev. B **77**, 134449 (2008).
- ⁹ C. Wu, K. Sun, E. Fradkin, and S. C. Zhang, Physical Review B **75**, 115103 (2007).
- ¹⁰ C. Wu, J. P. Hu, and S. C. Zhang, Phys. Rev. Lett. **91**, 186402 (2003).
- ¹¹ C. Wu, Phys. Rev. Lett. **95**, 266404 (2005).
- ¹² C. Wu, J. Hu, and S. Zhang, Int. J. Mod. Phys. B **24**, 311 (2010).
- ¹³ H.-H. Tu, G.-M. Zhang, and L. Yu, Phys. Rev. B **74**, 174404 (2006).
- ¹⁴ H.-H. Tu, G.-M. Zhang, and L. Yu, Phys. Rev. B **76**, 014438 (2007).
- ¹⁵ D. Zheng, G.-M. Zhang, T. Xiang, and D.-H. Lee, Phys. Rev. B **83**, 014409 (2011).
- ¹⁶ J. Zang, H.-C. Jiang, Z.-Y. Weng, and S.-C. Zhang, Phys. Rev. B **81**, 224430 (2010).
- ¹⁷ D. Lee, ArXiv e-prints (2010), 1009.4040.
- ¹⁸ E. Szirmai and M. Lewenstein, ArXiv e-prints (2010), 1009.4868.
- ¹⁹ D. Controzzi and A. M. Tsvelik, Phys. Rev. Lett. **96**, 97205 (2006).
- ²⁰ Y. Jiang, J. Cao, and Y. Wang (2010), 1006.2118.
- ²¹ K. Hattori, J. Phys. Soc. Jpn. **74**, 3135 (2005).
- ²² P. Lecheminant, E. Boulat, and P. Azaria, Phys. Rev. Lett. **95**, 240402 (2005).
- ²³ P. Lecheminant, P. Azaria, and E. Boulat, Nucl. Phys. B **798**, 443 (2008).
- ²⁴ D. Lee, Phys. Rev. Lett. **98**, 182501 (2007).
- ²⁵ A. V. Gorshkov, M. Hermele, V. Gurarie, C. Xu, P. S. Julianne, J. Ye, P. Zoller, E. Demler, M. D. Lukin, and A. M. Rey, Nature Phys. **6**, 289 (2010).
- ²⁶ M. Hermele, V. Gurarie, and A. M. Rey, Phys. Rev. Lett. **103**, 135301 (2009).
- ²⁷ C. Xu, Phys. Rev. B **81**, 144431 (2010).
- ²⁸ M. A. Cazalilla, A. F. Ho, and M. Ueda, New J. Phys. **11**, 103033 (2009).
- ²⁹ R. Flint, M. Dzero, and P. Coleman, Nat. Phys. **4**, 643 (2008).
- ³⁰ R. Flint and P. Coleman, Phys. Rev. B **79**, 014424 (2009).
- ³¹ A. K. Kolezhuk and T. Velua, ArXiv e-prints (2010), 1008.0598.
- ³² S. R. White, Phys. Rev. Lett. **69**, 2863 (1992).
- ³³ S. R. White, Phys. Rev. B **48**, 10345 (1993).
- ³⁴ K. I. Kugel' and D. I. Khomskii, Usp. Fiz. Nauk **136**, 631 (1982).
- ³⁵ B. Sutherland, Phys. Rev. B **12**, 3795 (1975).
- ³⁶ Y. Q. Li, M. Ma, D. N. Shi, and F. C. Zhang, Phys. Rev. Lett. **81**, 3527 (1998).
- ³⁷ M. V. D. Bossche, F. C. Zhang, and F. Mila, Eur. Phys. J. B **17**, 367 (2000).
- ³⁸ M. van den Bossche, P. Azaria, P. Lecheminant, and F. Mila, Phys. Rev. Lett. **86**, 4124 (2001).
- ³⁹ A. Mishra, M. Ma, and F. C. Zhang, Phys. Rev. B **65**, 214411 (2002).
- ⁴⁰ K. Harada, N. Kawashima, and M. Troyer, Phys. Rev. Lett. **90**, 117203 (2003).
- ⁴¹ N. Read and S. Sachdev, Phys. Rev. B **42**, 4568 (1990).
- ⁴² E. H. Lieb, T. Schultz, and D. J. Mattis, Ann. Phys. (N.Y.) **16**, 407 (1961).
- ⁴³ Y. Yamashita, N. Shibata, and K. Ueda, Phys. Rev. B **58**, 9114 (1998).
- ⁴⁴ P. L. P. Azaria, A. O. Gogolin and A. A. Nersesyan, Phys. Rev. Lett. **83**, 624 (1999).
- ⁴⁵ G. Fath, O. Legeza, and J. Solyom, Phys. Rev. B **63**, 134403 (2001).
- ⁴⁶ H.-H. Hung, C.-D. Gong, Y.-C. Chen, and M.-F. Yang, Phys. Rev. B **73**, 224433 (2006).
- ⁴⁷ I. Affleck, Nucl. Phys. B **265**, 409 (1986).
- ⁴⁸ G. M. Zhang and S. Q. Shen, Phys. Rev. Lett. **87**, 157201 (2001).

- ⁴⁹ F. Wang and A. Vishwanath, Phys. Rev. B **80**, 064413 (2009).
- ⁵⁰ S. Pankov, R. Moessner, and S. L. Sondhi, Phys. Rev. B **76**, 104436 (2007), URL doi:10.1103/PhysRevB.76.104436.
- ⁵¹ E. Dagotto and A. Moreo, Phys. Rev. B **39**, 4744 (1989).
- ⁵² Dagotto and A. Moreo, Phys. Rev. Lett. **63**, 2148 (1989).
- ⁵³ H. J. Schulz and T. A. L. Ziman, Europhys. Lett. **18**, 355 (1992).
- ⁵⁴ G. Santoro, S. Sorella, L. Guidoni, A. Parola, and E. Tosatti, Phys. Rev. Lett. **83**, 3065 (1999).
- ⁵⁵ L. Capriotti and S. Sorella, Phys. Rev. Lett. **84**, 3173 (2000).
- ⁵⁶ J. Richter and N. B. Ivanov, Czechoslovak J. Phys. **46**, 1919 (1996).
- ⁵⁷ Z. Ma, *Group Theory for Physicists* (World Scientific Publishing, 2008).